Microfabrication of large-area circular high-stress silicon nitride membranes for optomechanical applications

E. Serra, , M. Bawaj, , A. Borrielli, , G. Di Giuseppe, , S. Forte, , N. Kralj, , N. Malossi, , L. Marconi, , F. Marin, , F. Marino, , B. Morana, , R. Natali, , G. Pandraud, , A. Pontin, , G. A. Prodi, , M. Rossi, , P. M. Sarro, , D. Vitali, and , and M. Bonaldi

---

Articles you may be interested in

Silicon nitride membrane resonators at millikelvin temperatures with quality factors exceeding 10^8
Applied Physics Letters **107**, 263501 (2015); 10.1063/1.4938747

High quality mechanical and optical properties of commercial silicon nitride membranes
Applied Physics Letters **92**, 103125 (2008); 10.1063/1.2884191

Suppression of phonon tunneling losses by microfiber strings for high-Q membrane microresonators
Applied Physics Letters **109**, 191903 (2016); 10.1063/1.4967496

Nested trampoline resonators for optomechanics
Applied Physics Letters **108**, 033501 (2016); 10.1063/1.4939828

High-reflectivity, high-Q micromechanical membranes via guided resonances for enhanced optomechanical coupling
Applied Physics Letters **100**, 021110 (2012); 10.1063/1.3658731

Mechanically compliant grating reflectors for optomechanics
Applied Physics Letters **100**, 061124 (2012); 10.1063/1.3684248

Microfabrication of large-area circular high-stress silicon nitride membranes for optomechanical applications

E. Serra,[1,2] M. Bawaj,[3,4] A. Borrielli,[1,5] G. Di Giuseppe,[3,4] S. Forte,[2,6]
N. Kralj,[3] N. Malossi,[3,4] L. Marconi,[7,8] F. Marin,[7,8,9] F. Marino,[8,10] B. Morana,[2]
R. Natali,[3,4] G. Pandraud,[2] A. Pontin,[7,8] G. A. Prodi,[1,6] M. Rossi,[3]
P. M. Sarro,[2] D. Vitali,[3,4] and M. Bonaldi[1,5,a]

[1]*Istituto Nazionale di Fisica Nucleare, TIFPA, 38123 Povo (TN), Italy*
[2]*Delft University of Technology, Else Kooi Laboratory, 2628 Delft, The Netherlands*
[3]*Physics Division, School of Science and Technology, Università di Camerino,*
62032 Camerino (MC), Italy
[4]*INFN, Sezione di Perugia, 06123, Perugia, Italy*
[5]*Institute of Materials for Electronics and Magnetism, Nanoscience-Trento-FBK Division,*
38123 Povo (TN), Italy
[6]*Dipartimento di Fisica, Università di Trento, 38123 Povo (TN), Italy*
[7]*Dipartimento di Fisica e Astronomia, Università di Firenze, Via Sansone 1,*
50019 Sesto Fiorentino (FI), Italy
[8]*INFN, Sezione di Firenze, Via Sansone 1, 50019 Sesto Fiorentino (FI), Italy*
[9]*LENS, Via Carrara 1, 50019 Sesto Fiorentino (FI), Italy*
[10]*CNR-INO, L.go Enrico Fermi 6, 50125 Firenze, Italy*

In view of the integration of membrane resonators with more complex MEMS structures, we developed a general fabrication procedure for circular shape SiN_x membranes using Deep Reactive Ion Etching (DRIE). Large area and high-stress SiN_x membranes were fabricated and used as optomechanical resonators in a Michelson interferometer, where Q values up to 1.3×10^6 were measured at cryogenic temperatures, and in a Fabry-Pérot cavity, where an optical finesse up to 50000 has been observed. © *2016 Author(s). All article content, except where otherwise noted, is licensed under a Creative Commons Attribution (CC BY) license (http://creativecommons.org/licenses/by/4.0/).* [http://dx.doi.org/10.1063/1.4953805]

The optomechanical coupling between a laser beam and a microdevice via radiation pressure is of great interest in quantum-optics and fundamental research.[1] In fact, the latest micro- and nano-mechanical resonators, when used in a high-finesse Fabry-Pérot optical cavity, offer great potential for precision sensing[2,3] and for manipulation of the quantum state of light.[4,5]

In many cases the resonators consist of a free-standing high-stress silicon nitride (SiN_x) membrane supported by a silicon (Si) frame, where Q-frequency product above 10^{13} Hz can be obtained thanks to the large tensile stress (of the order of GPa).[6] These setups usually exploit dispersive coupling of the dielectric membrane placed in an optical cavity,[7] but there are a number of ongoing efforts to extend the capabilities of SiN_x membrane resonators, for instance by coating them with a metal for use in hybrid optical-microwave setups[8] or by enhancing optomechanical coupling by patterning of photonic crystal structures.[9] We also mention recent studies aiming to understand and possibly overcome the current limits in their mechanical performance.[10]

Large area free-standing SiN_x membranes were originally proposed as TEM windows. Generally, these are fabricated on a Si support by low pressure chemical vapour deposition (LPCVD) and then released by wet etching the Si substrate. For this last step potassium hydroxide (KOH) solutions are typically employed. However, this etching is highly selective along silicon crystal planes and allows precise control of dimensions only if the desired structure can be bounded by $< 111 >$ planes,[11] as in rectangular membranes. On the other hand the integration of the resonator in

---

[a]Corresponding author: bonaldi@science.unitn.it

complex microsystems requires a greater flexibility in terms of layout. We note that SiN_x membrane of arbitrary shape have been obtained by HF etching of a sacrificial SiO_2 layer,[12] but these devices are suspended over the silicon wafer and cannot be used in the membrane-in-the-middle cavity configuration, that is used for optomechanical experiments with semi-transparent membranes.

In this paper we describe a general fabrication procedure for opto-mechanical membranes based on Deep Reactive Ion Etching (DRIE) through-wafer etching. DRIE, that was already used to produce SiN membranes for filtration and separation,[13] allows the fabrication of membranes of any shape, because the design is not constrained by the crystal planes as in the case of KOH etching. At the same time it enables the fabrication of complex hybrid systems around the membrane. This is required to ease the integration of the SiN_x membrane with on-chip mechanical isolation, useful for improving the overall reproducibility of the resonator by reducing the mechanical coupling with the sample holder. We remark that this strategy has recently allowed the production of optomechanical microresonators where quality factors higher than 10^6 can reproducibly be obtained for specifically designed normal modes.[14,15] So far SiN_x resonators suspended from phononic band-gap isolation structures have been built by combining DRIE with a wet etch release of the SiN_x layer, but the process could not attain an optimal control of the membrane cleanliness.[16,17]

Membranes were fabricated following the steps shown in Figure 1(a)-1(j). As substrate we employed a double-side-polished Si wafer with a thickness of 500 μm and a RMS surface roughness lower than 1 nm. Prior fabrication the wafers were cleaned by immersing them in 99% HNO_3 and in 65% HNO_3 at 110 °C. A 200-nm-thick SiO_2 layer was then deposited by LPCVD using tetraethylorthosilicate (TEOS) as precursor [step(a)]. The LPCVD TEOS has a low compressive stress and works as etching stop layer during the DRIE etch. The fabrication followed with the LPCVD deposition of a 100-nm-thick SiNx layer [step (b)]. The deposition recipe was optimized for a residual tensile stress of about 1 GPa,[18] measured by wafer curvature (TENCOR Flexus FLX-2908). After the back-side etching [step (c)], a low-stress 1-μm-thick layer of pure Al was sputtered on the front side [step (d)]. This layer served to protect the SiN_x during the DRIE etch. A 6-μm-thick oxide layer was deposited on the backside by means of plasma enhanced chemical vapor deposition (PECVD) [step (e)]. Circular (square) holes with a diameter (side) up to 1.5 mm were patterned into this layer [step (f-g)]. The Si was then locally removed [step(h)] by means of DRIE (two pulse BOSCH process in Omega i2L Rapier). The etching rates were about 1.38 μm/cycle for Si and 5 nm/cycle for the PECVD oxide. Finally, the SiN_x membrane was released by first stripping the Al layer [step(i)] using a PES solution and then by etching the TEOS oxide [step (j)] by means of an HF-based solution. We point out that metal and oxide layers are only protective and do not concur in determining the shape. The etching of the silicon frame, that defines the membrane's shape, is fully realized by DRIE.

We focus the analysis of the mechanical resonance frequencies on the circular membranes, due to their original shape with respect to the more common square membranes. The theoretical resonance frequencies in a circular membrane are given by the expression $f_{mn} = f_0 \alpha_{mn}$ where α_{mn} is the n-th root of the Bessel polynomial of order m, and $f_0 = \frac{1}{2\pi} \sqrt{\frac{T}{\rho}} \frac{1}{R}$ (T is the stress, ρ the density, R the radius of the membrane). The modal shapes of the first $0n$ and $1n$ modes are shown in Figure 2.

We have measured the modal frequencies from a thermal spectrum acquired using a Michelson interferometer (Fig. 3), with the sample kept in a vacuum chamber. In Fig. 4(a) we show the experimental resonance frequencies divided by the respective α_{mn}, for the first $m = 0$ and $m = 1$ order modes. We expect a constant value, equal to f_0. It appears that the lower modes slightly (but systematically) deviate from the predicted behavior, with a maximum spread of just 4%, probably due to boundary effects, likely influenced by the clamping. We can extrapolate an asymptotic experimental value of $f_0 \simeq 114$ kHz, to be compared with $f_0 = 118.6$ kHz that is calculated using the nominal parameters $R = 0.75$ mm, $T = 1$ GPa and $\rho = 3200$ kg/m^3. The agreement is very good. We also remark that measurements taken at different times (entailing few degrees variations of the room temperature) yield fluctuations of the experimental f_0 by $2 - 3\%$.

An interesting property of the circular membrane is that the effective modal mass depends on the modal index, as opposed to the square membranes. Namely, the effective mass of the $0n$ modes for a centered, δ–like readout is $M_{0n} = M(J_1(\alpha_{0n}))^2$, where M is the physical mass of the membrane and J_m is the Bessel polynomial (the first values of M_{0n}/M are 0.269, 0.116, 0.074, 0.054,
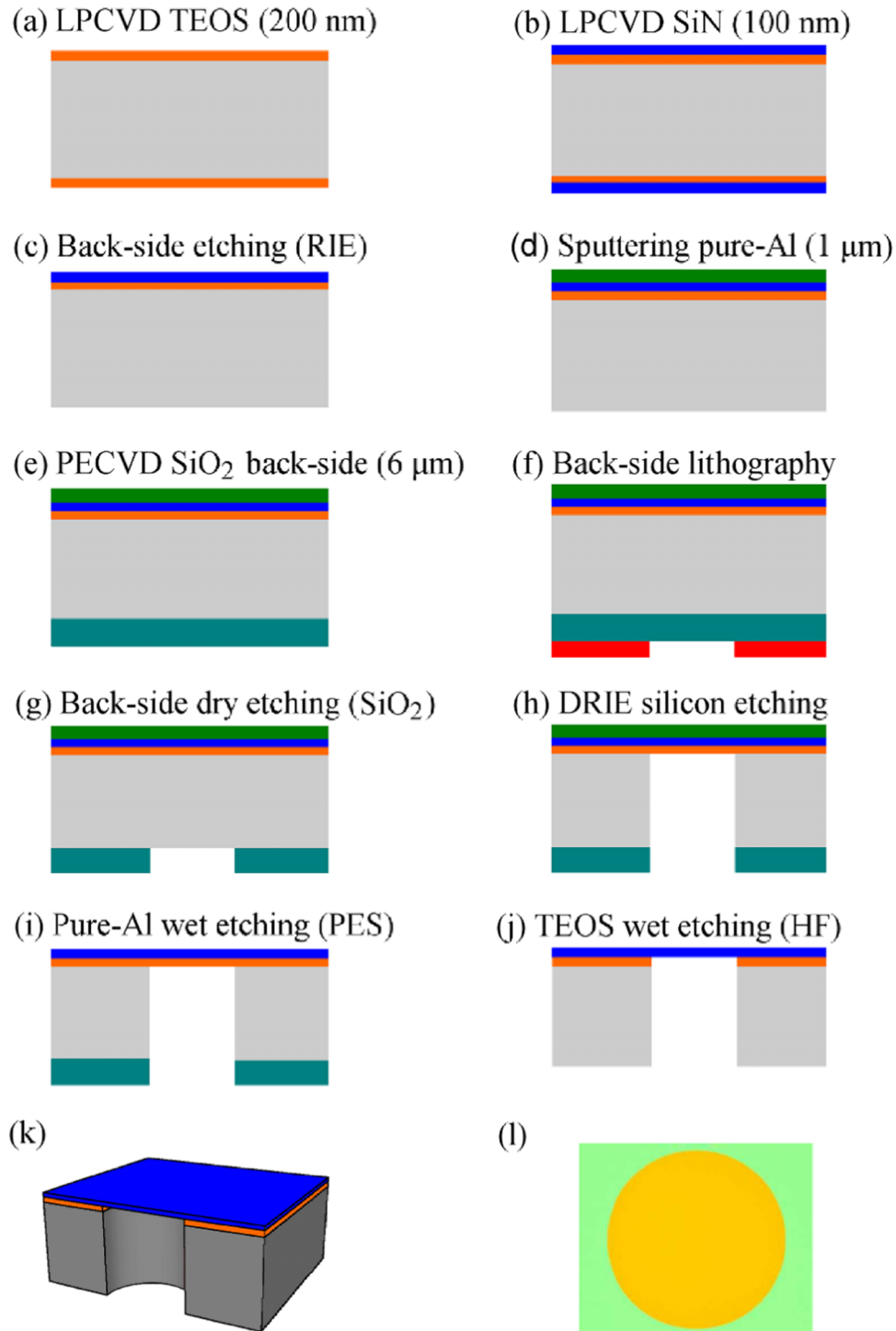
FIG. 1. (a)-(j) Fabrication steps. (k) Section view of the finished device. (l) Optical microscope image of a circular membrane of diameter 1.5 mm.

0.043). The mass is lower at higher index because the modal displacement is more concentrated in the center, while it remains homogeneous for a square membrane. For comparison, in the case of a square membrane the effective mass of the odd modes is $M/4$. A reduced effective mass, increasing the susceptibility, is a useful property in opto-mechanics experiments. In the realistic case of a
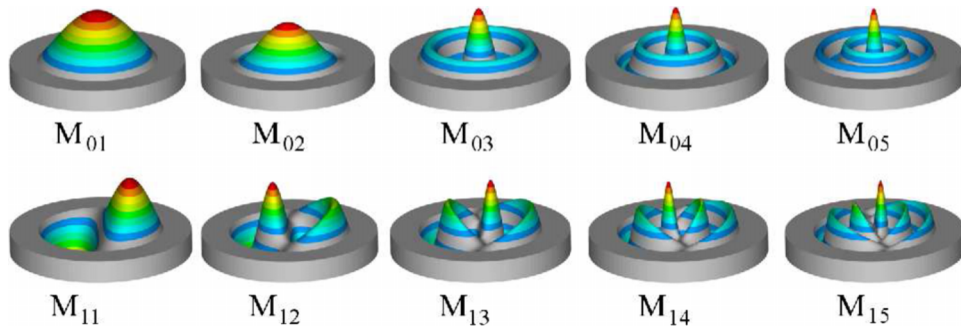
FIG. 2. Modal shape of the first $0n$ and $1n$ modes of a circular membrane. The color scale, from light gray to red, is proportional to the absolute displacement from the equilibrium position.

centered, Gaussian readout with $1/e^2$ width w, the effective mass becomes:

$$M_{0n} = M \left(\frac{J_1(\alpha_{0n})}{\frac{4}{w^2} \int J_0(\alpha_{0n}r/R) \exp\left(-\frac{2r^2}{w^2}\right) r\,\mathrm{d}r} \right)^2 . \tag{1}$$

In Fig. 4(b) we report the experimental values of M_{0n} for the first modes, derived from the areas A_{0n} of the thermal peaks in the displacement spectrum using $A_{0n} = \frac{k_B \mathrm{T}_K}{M_{0n}(2\pi f_{0n})^2}$ (k_B is the Boltzmann constant and T_K the temperature). They are compared with the theoretical values calculated for a realistic $w = 0.15$ mm (showing a good agreement) and with a pointlike readout.

We have verified by Finite Element (FE) analysis that the expected quality factor is similar to that of a square membrane with the same modal frequency of the first mode. In fact, for each mode, a FE routine can evaluate the energy stored in different parts of the systems and can estimate the overall quality factor from the loss angle assigned to each part.[19] To validate our procedure we have verified (Figure 5(a)) that the quality factors of the modes of the square membrane evaluated by FE are in good agreement with the values expected from the theory. For a square membrane of side 1.52 mm, thickness 100 nm and internal stress 1 GPa, the quality factor envelope can been evaluated as:[20]

$$Q_{square} \simeq \frac{1.1 \times 10^7}{1 + 1.35 \times 10^{-13} f^2} \tag{2}$$

where f is the frequency of the modes and the intrinsic loss has been set as $1/Q = 2 \times 10^{-3}$, the room temperature value.[10] The case of a circular membrane is then solved with the same FE routine, obtaining quite similar values (Fig. 5(a)). Note that the loss ($1/Q$) grows with the frequency because higher order modes have an increasing number of nodal lines.

The simulation can take into account also the loss from the substrate supporting the membrane, that has not been obtained in closed form yet. In fact the borders of the membrane bends during the oscillation and the first layer of the substrate is subjected to a mechanical strain. This contribution is
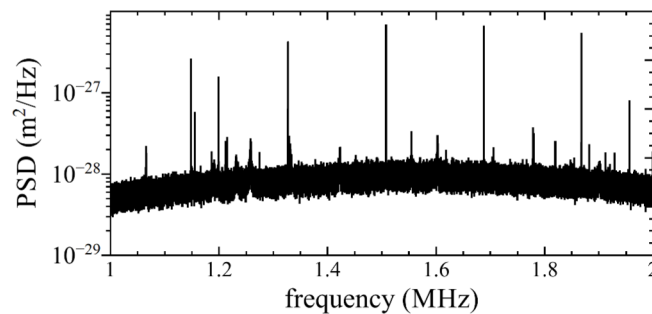

FIG. 3. Typical noise power spectral density (PSD) of the interferometer output; the modal frequencies can be clearly seen above background noise.
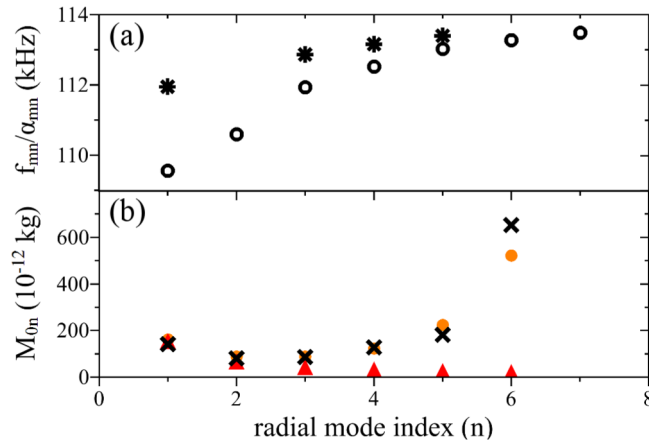
FIG. 4. (a) Resonance frequencies of the first $0n$ (open circles) and $1n$ (stars) modes af a $R = 0.75$ mm circular membrane, divided by the respective α_{mn}. (b) Experimental effective mass M_{0n} of the first modes (crosses), theoretical values calculated for a centered Gaussian readout with width $w = 0.15$ mm (closed circles) and for a pointlike readout (triangles).

negligible when the SiN$_x$ layer is directly grown on silicon, but it may become relevant in our case, as the membrane is grown over a SiO$_2$ layer. At room temperature the loss angle of SiO$_2$ is as low as $1/Q = 5 \times 10^{-5}$ and we have not found an additional contribution.[21] At liquid helium temperature the expected loss[22] for SiN$_x$ reduces to $1/Q = 2 \times 10^{-5}$, while for SiO$_2$ it grows to $1/Q = 7 \times 10^{-4}$. In this case the substrate becomes the main source of loss and limits the maximum quality factor to 5×10^6, as shown in Figure 5(b). We note here that the loss is set by the contribution of the border and the frequency dependence can no longer be seen in the simulation data. We point out that these results are necessarily approximate, as the intrinsic loss angle value can be strongly dependent on the deposition procedure or on the thickness of the adhesion layer.[22]

The mechanical quality factor Q of the modes of different membranes has been measured both at room and at cryogenic temperatures, by driving the different resonances with a piezoelectric glued on the sample mount, and observing the ring-down with a Michelson interferometer. At room temperature, the Q values are very scattered, ranging from few thousands up to 2×10^5. This feature is very common in SiN$_x$ membranes, and is due to the coupling with the frame and, through it, with the sample holder. At cryogenic temperatures, the values of Q are still scattered, but globally higher. With a 1.5 mm diameter membrane on a 5 mm side, square frame clamped between two copper plates, we could measure a maximum Q of 0.65×10^6, at 8 K. With a 1 mm side, square membrane close to the edge of a 5×20 mm^2 frame, glued on the opposite edge to a copper block, we could measure Q values up to 1.3×10^6 at 13 K. As we aim to develop a general-purpose device, with
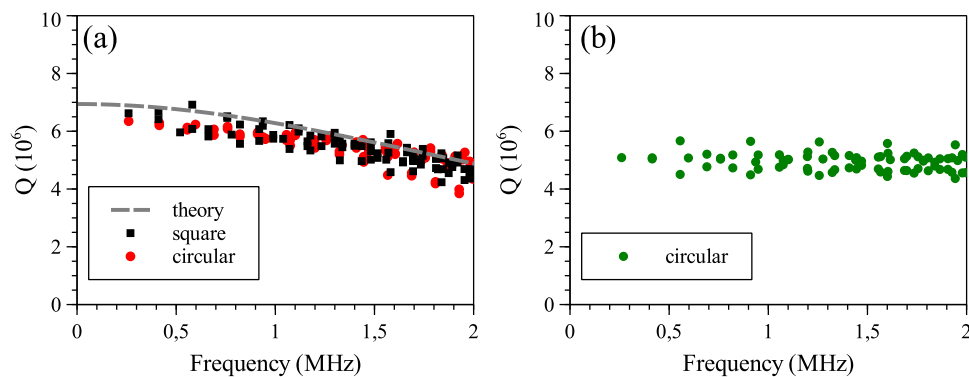

FIG. 5. Finite Elements estimate of quality factor of tensioned membranes. (a) Room temperature simulations for a square membrane (squares) with side 1.52 mm and for our circular membrane (closed circles). The dashed line is the theoretical prediction Eq. (2) for the square membrane. (b) Low temperature simulation for the circular membrane. Here the quality factor is limited by the SiO$_2$ adhesion layer.

features independent from the details of the experimental apparatus, we did not optimize the efforts to improve the best measured quality factor by trying different mounting systems. We also note that, even if the meaningful clamping losses do not permit a better assessment, the FEM calculations indicate that the loss from the SiO_2 adhesion layer limits the expected Q for membranes of our size to about 5×10^6 (Figure 5(b)). In this context, we estimate that a Q higher than 10^6 it is enough to motivate the future development of on-chip isolation system for these membranes.

We characterized the optical properties of a circular membrane of nominal radius $R = 0.6$ mm, with thickness $L_d = 97.27 \pm 0.01$ nm and index of refraction at $\lambda = 1064$ nm $n_R = 2.0210 \pm 0.0005$, measured during production [step (b)] by variable angle spectroscopic ellipsometry (VASE). These values have been confirmed by polarization-resolved transmission measurements again at $\lambda = 1064$ nm, performed on the final, diced samples. These latter measurements provide an intensity reflectivity at normal incidence $|r_d|^2 = 0.355 \pm 0.002$, perfectly consistent with the expression for the amplitude reflection and transmission coefficients of a dielectric membrane of thickness L_d and refractive index n,

$$r_d = \frac{(n^2 - 1)\sin\beta}{2in\cos\beta + (n^2 + 1)\sin\beta},$$ (3)

$$t_d = \frac{2n}{2in\cos\beta + (n^2 + 1)\sin\beta},$$ (4)

where $\beta = nkL_d = 2\pi nL_d/\lambda$. When $n = n_R$ is real there is no optical absorption, but in general $n = n_R + in_I$, with the small but nonzero imaginary part n_I providing a measure of optical absorption. In order to accurately evaluate it, we have placed the membrane between two Al cylinders, and we have inserted it in a $L = 9.03$ cm long cavity at room temperature formed by two spherical mirrors of radius of curvature 7.5 cm. The high-frequency component of the Pound-Drever-Hall (PDH) signal used to lock the cavity was acquired for the preliminary analysis of the mechanical modes at a vacuum chamber pressure of 1.7×10^{-2} mbar. The fundamental eigenfrequency is found to be $f_{01} \sim 348.5$ kHz, consistent with the theoretical expectation if we assume $R = 0.615$ mm. The detected optical cavity modes as a function of the membrane position are also consistent with the theoretical model obtained with the cavity and membrane parameters.[23,24] Finally the cavity finesse, $\mathcal{F}_T$, as a function of the membrane position has been measured (see Fig. 6) by the ringdown technique. The laser beam, deflected by an acousto-optic-modulator (AOM) and sent into the cavity, is switched off in 50 ns after the transmitted light has reached a threshold level. The leakage of transmitted light is monitored to estimate the cavity decay-time, which is fitted with a single exponential form whose time constant, τ, is related to $\mathcal{F}_T$ via $\mathcal{F}_T = \pi c\tau/L$. Repeating the finesse measurement for different positions of the membrane as reported in Fig. 6, allows to estimate n_I and the roughness of the membrane. For fitting the finesse data we consider the transfer function of a cavity with a membrane in the middle. The cavity consists of two semi-cavities; denoting with z the position of the membrane with respect to the cavity center, and assuming for the reflection and transmission coefficients of the mirrors $r_1 = r_2 = \sqrt{\mathcal{R}}$ and $t_1 = t_2 = \sqrt{\mathcal{T}}$, we derive the following expression for the intensity transmission:

$$\mathcal{T}_c = \frac{|\mathcal{T} t_d|^2}{\left|1 + 2r_d\sqrt{\mathcal{R}}\cos(2kz)e^{ikL} + \mathcal{R}(t_d^2 + r_d^2)e^{2ikL}\right|^2}.$$ (5)

In the ideal case $\mathcal{R} = 1$ and n is real, so that $t_d^2 + r_d^2 = \exp\{2i\arg(r_d)\} = \exp\{2i\phi_r\}$, the eigenfrequencies of the cavity modes are given by the zeros of the denominator of the cavity transmission $[\cos(kL + \phi_r) + |r_d|\cos(2kz)]^2 = 0$, which gives the results in Ref. 24

$$2kL = \nu\frac{2\pi}{\Delta\nu_{FSR}} = -2\phi_r + 2\cos^{-1}[-|r_d|\cos(2kz)].$$ (6)

When $\mathcal{R} < 1$ and in the presence of absorption the resonance frequencies of the cavity modes are determined by the maxima of the transmission $\mathcal{T}_c$ given by Eq. (5), and the finesse can be obtained from the width of the transmission peaks. Roughness can be introduced following Refs. 25–27, according to which any optical element with a given roughness is responsible for a modification of the
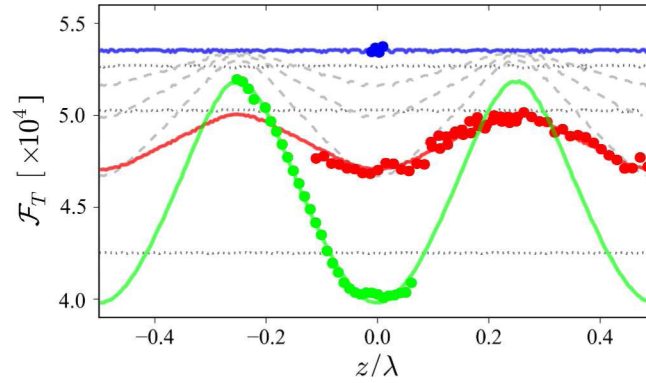
FIG. 6. Plot of the cavity finesse, $\mathcal{F}_T$ versus membrane position along the cavity axis. Red-symbols represent data for a circular-membrane, 1.2 mm diameter, and 97 nm thickness. Red-line represents the best fit with fitting parameters $\bar{n}_I$ = $(1.97 \pm 0.08) \times 10^{-6}$ and $\bar{\sigma}_{opt}$ = (287 ± 4) pm, and with the following fixed parameters: the membrane thickness L_d = 97 nm, the real part of the refractive index n_R = 2.021, the cavity length L = 9.03 cm, the wavelength λ = 1064 nm, and the empty-cavity finesse $\mathcal{F}_v$ = 53500 ± 100, which is evaluated as mean value of the data shown as blue-symbols. Green-symbols represent data for a square-membrane, 1 mm side, 50 nm thickness by Norcada, The green-line is the fitting with parameters n_I = $(1.0 \pm 0.01) \times 10^{-5}$ and σ_{opt} = (280 ± 10) pm. Dashed-gray (dotted-gray) curves represent theoretical expectation for the circular membrane with parameters fixed as σ_{opt} = 0 (n_I = 0) and $n_I/\bar{n}_I$ = .5, 1, 2 ($\sigma_{opt}/\bar{\sigma}_{opt}$ = .5, 1, 2), from upper to lower curve. They demonstrate the different contribution of absorption and roughness to the finesse behaviour upon membrane position.

wavefront and therefore leads to a scattering loss from the incident optical mode into all the other cavity modes. This scattering into other modes induced by an effective optical roughness σ_{opt} can be modeled by including a factor $\sqrt{\exp[-(2k\sigma_{opt})^2]}$ multiplying r_d in eq. (3). Fig. 6 shows the best fits for the set of data (red symbols) taken for the 1.2 mm–diameter circular membranes. We have taken n_I and σ_{opt} as fitting parameters, while we have kept fixed all the other parameters (L_d = 97 nm, n_R = 2.021, L = 9.03 cm, λ = 1064 nm, and $\mathcal{F}_v$ = 53500 ± 100 corresponding to $\mathcal{R}$ = 0.9999413). While the $\lambda/2$ periodicity is caused by the absorption which is maximum at the antinodes and minimum at the nodes of the cavity field, the membrane roughness causes scattering which instead does not significantly depend upon the membrane axial position (as shown in Fig. 6). The fit gives an imaginary part of the refractive index $\bar{n}_I$ = $(1.97 \pm 0.08) \times 10^{-6}$ and $\bar{\sigma}_{opt}$ = (287 ± 4) pm. As a comparison, the results for a 1 mm side, 50 nm thickness membrane by Norcada[28] are reported with fitting parameters n_I = $(1.00 \pm 0.01) \times 10^{-5}$ and σ_{opt} = (280 ± 10) pm. The circular membranes we fabricated present a similar effective optical roughness with respect to a commercial square one but a lower absorption. As regards standard AFM measurement of roughness, we measured for our membranes σ_{rms} = 0.7 ± 0.1 nm over scan areas of $1 \mu m \times 1 \mu m$.

In conclusion, we developed and validated a general fabrication procedure for free-standing large area high-stress SiN_x membranes of any shape with a good dimensional precision by using DRIE etching. Possible improvements of the process could be obtained by the use of silicon substrates with a lower initial roughness. This work is a crucial step toward the integration of SiN_x membranes in hybrid systems and on-chip mechanical isolation.

We mention that some interesting development have been recently reported,[29,30] published after the submission of this work. Here small membranes (about $100 \times 100 \ \mu m^2$) are supported by trampolines that act as flexure elements, and demonstrate the effectiveness of a careful engineering in obtaining high quality factors. These resonators also have a very small mass, obtained at the expense of a reduced heat management capability, and therefore target different experimental regimes compared to large membranes.

[1] M. Aspelmeyer, T.J. Kippenberg, and F. Marquardt, Rev. Mod. Phys. **86**, 1391 (2014).

[2] T.P. Purdy, R.W. Peterson, and C.A. Regal, Science **339**, 801 (2013).

[3] M. Bawaj, C. Biancofiore, M. Bonaldi, F. Bonfigli, A. Borrielli, G. Di Giuseppe, L. Marconi, F. Marino, R. Natali, A. Pontin, G.A. Prodi, E. Serra, D. Vitali, and F. Marin, Nat. Commun. **6**, 7503 (2015).

[4] A.H. Safavi-Naeini, S. Groblacher, J.T. Hill, J. Chan, M. Aspelmeyer, and O. Painter, Nature **500**, 185 (2013).

[5] T.P. Purdy, P.-L. Yu, R.W. Peterson, N.S. Kampel, and C.A. Regal, Phys. Rev. X **3**, 031012 (2013).

[6] D.J. Wilson, C.A. Regal, S.B. Papp, and H.J. Kimble, Phys. Rev. Lett. **103**, 207204 (2009).

[7] J.D. Thompson, B.M. Zwickl, A.M. Jayich, Florian Marquardt, S.M. Girvin, and J.G.E. Harris, Nature **452**, 72-75 (2008).

[8] R.W. Andrews, R.W. Peterson, T.P. Purdy, K. Cicak, R.W. Simmonds, C.A. Regal, and K.W. Lehnert, Nat. Phys. **10**, 321326 (2014).

[9] Catvu H. Bui, Jiangjun Zheng, S. W. Hoch, Lennon Y. T. Lee, J. G. E. Harris, and Chee Wei Wong, Appl. Phys. Lett. **100**, 021110 (2012).

[10] L.G. Villanueva and S. Schmid, Phys. Rev. Lett. **113**, 227201 (2014).

[11] C.T. Leondes, *Mems/Nems Handbook* (Springer, 2006).

[12] D. R. Southworth, R. A. Barton, S. S. Verbridge, B. Ilic, A. D. Fefferman, H. G. Craighead, and J. M. Parpia, Phys. Rev. Lett. **102**, 225503 (2009).

[13] P. Galambos, K. Zavadil, R.J. Shul, C. Lober Willison, and S.L. Miller, Proc. SPIE 3877, Microfluidic Devices and Systems II, 273 (1999).

[14] E. Serra, A. Borrielli, F. S. Cataliotti, F. Marin, F. Marino, A. Pontin, G. A. Prodi, and M. Bonaldi, Appl. Phys. Lett. **101**, 071101 (2012).

[15] A. Borrielli, A. Pontin, F. S. Cataliotti, L. Marconi, F. Marin, F. Marino, G. Pandraud, G. A. Prodi, E. Serra, and M. Bonaldi, Phys. Rev. Applied **3**, 054009 (2015).

[16] P.-L. Yu, K. Cicak, N.S. Kampel, Y. Tsaturyan, T.P. Purdy, R.W. Simmonds, and C.A. Regal, Appl. Phys. Lett. **104**, 023510 (2014).

[17] Y. Tsaturyan, A. Barg, A. Simonsen, L.G. Villanueva, S. Schmid, A. Schliesser, and E.S. Polzik, Opt. Express **22**, 6810 (2014).

[18] P.J. French, P.M. Sarro, R. Mallée, E.J.M. Fakkeldij, and R.F. Wolffenbuttel, Sens. Actuators A **58**, 149 (1997).

[19] E. Serra, M. Bonaldi, A. Borrielli, L. Conti, G. Pandraud, and P.M. Sarro, Sensors and Actuators A: Physical **227**, 48 (2015).

[20] P.-L. Yu, T. P. Purdy, and C. A. Regal, Phys. Rev. Lett. **108**, 083603 (2012).

[21] M. Principe, I.M. Pinto, V. Pierro, R. DeSalvo, I. Taurasi, A.E. Villar, E.D. Black, K.G. Libbrecht, C. Michel, N. Morgado, and L. Pinard, Phys. Rev. D **91**, 022005 (2015).

[22] X. Liu, T.H. Metcalf, Q. Wang, and D.M. Photiadis, Mater. Res. Soc. Symp. Proc. **989**, A22-01 (2007).

[23] C. Biancofiore, M. Karuza, M. Galassi, R. Natali, P. Tombesi, G. Di Giuseppe, and D. Vitali, Phys. Rev. A **84**, 033814 (2011).

[24] A.M. Jayich, J.C. Sankey, B.M. Zwickl, C. Yang, J.D. Thompson, S.M. Girvin, A.A. Clerk, F. Marquardt, and J.G.E. Harris, New J. Phys. **9**, 095008 (2008).

[25] D. Kleckner, W.T.M. Irvine, S.S.R. Oemrawsingh, and D. Bouwmeester, Phys. Rev. A **81**, 043814 (2010).

[26] W. Winkler, R. Schilling, K. Danzmann, J. Mizuno, A. Rüdiger, and K.A. Strain, Appl. Opt. **33**, 7547 (1994).

[27] The Virgo collaboration, *The VIRGO physics book*, Vol. II, available online at http://www.virgo-gw.eu/vpb/.

[28] Norcada Inc., http://www.norcada.com.

[29] C. Reinhardt, T. Müller, A. Bourassa, and J.C. Sankey, Phys. Rev. X **6**, 021001 (2016).

[30] R.A. Norte, J.P. Moura, and S. Gröblacher, Phys. Rev. Lett. **116**, 147202 (2016).